American Mineralogist, Volume 80, pages 1145–1156, 1995

Single-crystal IR spectroscopy of grossular-andradite garnets

B. P. McAloon
Department of Geology, University of California, Davis, California 95616, U.S.A.
A. M. Hofmeister
Department of Earth and Planetary Sciences, Washington University, St. Louis, Missouri 63131, U.S.A.

Abstract

Fe^{3+}-Al^{3+} substitution in the octahedral site of 14 natural garnet samples was investigated through measurement of complete single-crystal infrared (IR) reflectance spectra across the grossular-andradite [$Ca_3(Al_xFe_{1-x})_2Si_3O_{12}$] binary. Frequencies of all 17 IR-active fundamental modes depend nearly linearly on composition. Two peaks assigned to translations of the octahedral cations against the O framework exhibit two-mode behavior. Observation of similar frequencies for bands involving Al and Fe^{3+} and of much larger intensities for bands associated with Fe^{3+} suggests that the Fe-O bond has greater strength, which compensates for the greater mass of Fe. The nearly linear behavior of the modes indicates that mixing should approach ideality for this series, as was previously observed in thermodynamic studies. The existence of ideal mixing suggests that high degrees of ordering are not present, and thus that ordering might not cause the anomalous birefringence associated with this series.

Introduction

The garnet structure (e.g., Novak and Gibbs, 1971) is ideal for the study of solid-solution behavior of vibrational modes owing to its high (i.e., cubic) symmetry and to the variety of chemical substitutions possible. Spectroscopic studies of solid solutions are motivated by (1) the observation that macroscopic properties vary nonlinearly with some compositional series (e.g., Ganguly and Saxena, 1987), (2) the existence of models that allow for calculation of macroscopic properties from microscopic behavior (e.g., Kieffer, 1979), and (3) the insight provided by infrared (IR) vibrations into the nature of the chemical bond. The grossular-andradite [$Ca_3(Al_xFe_{1-x})_2Si_3O_{12}$] binary is of interest because for this series the bulk modulus appears to be nonlinear (Bass, 1986), yet shear modulus (Bass, 1986) and lattice parameter depend almost linearly on composition (Huckenholz et al., 1974), and other experimental and theoretical studies suggest essentially ideal mixing (e.g., Holdaway, 1972; Ganguly, 1976; Perchuk and Aranovich, 1979; Bird and Helgeson, 1980).

Previously, McAloon and Hofmeister (1993) obtained spectra from three end-member samples and an intermediate, upon which crystallographic refinements had been performed, to investigate the effect of ordering on IR spectra of garnets. This study presents complete IR reflectance data for 14 natural samples that lie close to or on the grossular-andradite (Gr-An) binary. Natural samples were used despite some uncertainties in the site occupancy, because reflectance measurements from single crystals are complete and quantitative. It is not necessary to obtain absorption spectra because these data can be extracted from reflectance spectra (e.g., Wooten, 1972). Frequencies of the 17 garnet IR-active fundamentals (lattice vibrations) depend approximately linearly on composition, which is consistent with ideal mixing.

Experimental methods

Compositional analyses were obtained with a Cameca SX-50 electron microprobe using a 15 keV acceleration voltage, 20 nA sample current, and 40 s counting times. Natural mineral standards were used. Compositional maps based on microprobe data were drawn for samples displaying zonation; such samples were used for IR measurements only if a homogeneous area of at least 150 × 150 μm existed.

Infrared reflectance spectra were obtained at ambient temperature and 1.0 or 2.0 cm^{-1} resolution using an evacuated Bomem DA3.02 Fourier Transform Interferometer (FTIR) equipped with a mercury cadmium telluride detector and a KBr beamsplitter for the range 450–4000 cm^{-1} and with a Si bolometer and various Mylar beamsplitters for wavelengths below 600 cm^{-1}. Spectra were collected from singly polished samples with random crystal orientation and sizes ranging from ~0.25 × 0.25 × 0.03 mm to ~12.0 × 14.0 mm using a Spectratech FTIR microscope. Doubly polished sections were not used to avoid multiple reflections. A Kramers-Kronig analysis (e.g., Andermann et al., 1965) was performed on merged reflectance spectra [see Hofmeister and Chopelas (1991) for procedural details]. Longitudinal optic (LO) peak positions were obtained from minima in the imaginary part of the dielectric function $\mathrm{im}[1/(\epsilon_1 + i\epsilon_2)]$, and transverse optic (TO) peak positions were obtained from maxima in the dielectric function ϵ_2. Absorptivity was calculated from

0003–004X/95/1112–1145$02.00

Table 1. Sample descriptions

Sample	Approx. comp.	Color of hand sample	Retardation* (mμm)	Thickness (mm)	Birefringence*	Locality	Source, cat. no.**
43	$Gr_{1.5}An_{98.5}$	yellow-green	950	0.658	0.001 undulatory	Stanley Butte, Graham Co., AZ	1, bulk
19	Gr_6An_{94}†	dk. brown			0.005†	Sonoma Mt. Range, NV	2†
33	Gr_8An_{92}	green-brown	50	0.01	0.005 spotty	Franklin, NJ	3, 9925
25	$Gr_{11.7}An_{88.3}$‡	green	1700	0.697	0.002 spotty	Santa Rita Peak, San Benito Co., CA	3, 24144
41	$Gr_{12.2}An_{87.8}$‡	yellow-green	1100	0.284	0.004 spotty	Clear Creek, San Benito Co., CA	1, bulk
44	$Gr_{29}An_{71}$	green	1100	0.395	0.003 spotty	Darwin Mine District, Inyo Co., CA	4, DA593
52	$Gr_{39}An_{61}$	pale green	cloudy§	0.897	0.01	Darwin Mine District, Inyo Co., CA	4, 203
35	$Gr_{49}An_{51}$	dk. brown	deep color§	0.871	§	Garnet Hill, Calaveras Co., CA	3, bulk
M	$Gr_{64}An_{36}$‖	green			0.01‖	Munam, North Korea	5, GRR1411
27	$Gr_{71}An_{29}$	dk. brown	deep color§	1.535	§	Bishop, Inyo Co., CA	3, 5183
28	$Gr_{80}An_{20}$	lt. brown, orange	330	0.841	0.0004 undulatory	Mussa Alp, Piedmont, Italy	3, 5153
51	$Gr_{91}An_9$	white, colorless	300	1.073	0.0003 spotty	Lake Jaco, Mexico	6, SM888
24	$Gr_{95}An_5$	white, colorless	1100	1.089	0.001 undulatory	Cerro los Muertos, Chihuahua, Mexico	3, bulk
12	$Gr_{99}An_1$#	white, colorless	160	0.540	0.0003 undulatory	Asbestos, Quebec, Canada	7#

Note: Compositions are normalized to end-members $(Ca^{2+},Mn^{2+},Fe^{2+},Mg^{2+})_3Al_2(Si,Ti)_3O_{12}$-$Ca_3(Fe^{3+},Cr^{3+})_2(Si,Ti)_3O_{12}$. See text for discussion.

* Retardation and birefringence are average values from unoriented samples. Birefringence value for sample 52 is from Eastman (1980).

** Source references are as follows: 1 = J. de Mouthe, California Academy of Sciences, San Francisco, CA; 2 = J. Downs, Ohio State University, Columbus, OH (sample obtained from Ernest G. Ehler's personal collection at Ohio State University); 3 = A. Kampf and D. Eatough, Los Angeles County National History Museum, Los Angeles, CA; 4 = H. Eastman, Bond Gold, Denver, CO (a description of the sample is given by Eastman, 1980); 5 = G. Rossman, California Institute of Technology, Earth and Planetary Sciences Division, Pasadena, CA; 6 = University of California, Davis, CA; 7 = F. Allen, Engelhard Corporation, Edison, NJ. Uncataloged materials are referred to by "bulk."

† Kingma and Downs (1989).

‡ More figures are reported than are significant to differentiate samples 25 and 41.

§ These samples were too darkly colored or opaque (cloudy) with fluid inclusions to ascertain retardation.

‖ G.R. Rossman (personal communication). See also Takeuchi et al. (1982) and Rossman and Aines (1991).

Allen and Buseck (1988).

$$\alpha(\nu) = 2\pi\nu\epsilon_2(\nu)/n(\nu) \quad (1)$$

where α is absorptivity, n is the index of refraction (calculated from the reflectivity; see, e.g., Wooten, 1972), and ν is frequency. An ambient-temperature, deuterated triglycine sulfate detector and a 6 or 12 μm Mylar beamsplitter were used to obtain supplementary far-IR absorption data from powder dispersed in petroleum jelly on a polyethylene card. Uncertainties in peak positions of ± 1–0.01 cm^{-1} are related to peak widths (or estimations of shoulder positions) because the accuracy of the FTIR spectrometer is an order of magnitude smaller.

Crystals were polished and examined with a petrographic microscope. Average optical retardation (Δ in units of 10^{-6} mm) was estimated visually by comparison with a Michel-Levy interference color chart. Because of the variable and undulatory nature of birefringence, a more precise quantitative measurement of the small amounts of retardation using a Berek compensator was not possible. Birefringence (δ) was calculated with the formula

$$\delta = n_2 - n_1 = 10^6\Delta/t \quad (2)$$

(e.g., Kerr, 1977), where n is the index of refraction and t is the thickness in millimeters. Thicknesses were measured with a digital micrometer.

Chemical composition

Fifty-two natural single crystals were obtained from the individuals listed in Table 1 and in the Acknowledgments or from the University of California, Davis, collection. Only samples with minimal (<3% total) pyrope-almandine-spessartine $[(Mg,Fe,Mn)_3Al_2Si_3O_{12}]$ and uvarovite $(Ca_3Cr_2Si_3O_{12})$ components were used for IR study. Fourteen of the samples (Table 1) met these criteria and adequately covered the grossular-andradite binary. Average chemical analyses are reported in Table 2. [Previously published analyses are summarized in Table 1. The Munam sample is slightly off the binary with a reported composition of $(Ca_{2.91}Mn_{0.05}Fe^{2+}_{0.04})(Al_{1.33}Fe^{3+}_{0.65}Ti_{0.02})(Si_{2.97}Al_{0.03})O_{12}$: Takeuchi et al., 1982.] Individual microprobe analyses and data for the other samples may be obtained from the authors. One of the 14 samples investigated may be problematic: sample 25 is Si deficient and has a low total weight percent.

Small amounts of H have been detected in samples from some of the same localities investigated here. From the study of Rossman and Aines (1991), it is probable that sample 51 has 0.04 wt% H_2O, M has 0.08 wt%, 24 has 0.11 wt%, 44 and 52 have 0.20 wt%, 28 has 0.37 wt% H_2O, and 12 has 0.08–0.38 wt% H_2O. From the study of

TABLE 2. Average microprobe analyses

Sample	43	33	25	41	44	52	35	27	28	51	24
Points sampled	9	62	23	4	3	3	43	53	31	10	14
Oxides (wt%)*											
SiO_2	34.94(15)	35.07(20)	33.07(30)	34.44(36)	36.32(39)	36.10(8)	37(9)	37.50(48)	38.34(24)	38.93(15)	39.73(24)
TiO_2	0.02(2)	0.10(5)	0.02(2)	0.06(6)	0.69(25)	0.38(14)	0.61(16)	0.78(12)	0.50(13)	0.70(10)	0.01(3)
Al_2O_3	0.31(22)	1.58(26)	2.45(12)	2.53(15)	5.96(96)	8.31(45)	10(2)	15.56(26)	17.42(41)	20.13(20)	20.89(17)
Cr_2O_3	0.02(3)	0.01(2)	0.01(2)	0.02(2)	0.03(2)	0.03(2)	0.03(4)	0.03(3)	0.01(2)	0.01(1)	0.01(2)
Fe_2O_3	30.75(29)	28.92(47)	27.55(21)	27.33(19)	22(1)	19.58(76)	15(4)	8.56(45)	6.42(59)	3.15(17)	1.78(30)
MgO	0.03(2)	0.03(2)	0.19(3)	0.175(5)	0.14(8)	0.10(3)	0.08(3)	0.06(2)	0.23(6)	0.81(8)	0.37(3)
CaO	32.34(23)	33.01(31)	34.05(21)	32.90(44)	32.76(22)	34.74(18)	33(5)	34.06(38)	35.49(40)	37.11(18)	37.02(31)
MnO	0.15(5)	0.73(31)	0.06(6)	0.02(4)	0.44(3)	0.35(9)	0.76(22)	1.12(19)	0.33(7)	0.10(2)	0.08(8)
FeO**	1.03(36)	0.22(26)	1.23(36)	0.98(34)	0.47(43)	0.87(13)	0.7(5)	1.35(38)	0.40(31)	0.04(5)	0.00(0)
Total	99.57(69)	99.69(56)	98.62(59)	98.46(27)	98.76(24)	100.46(24)	97.28(58)	99(1)	99.13(49)	100.97(39)	99.90(39)
Cations†											
Si	5.953	5.929	5.692	5.876	6.007	5.854	6.030	5.919	5.957	5.871	6.007
Ti	0.003	0.012	0.002	0.007	0.086	0.046	0.075	0.093	0.058	0.096	0.002
Al	0.063	0.316	0.497	0.508	1.161	1.589	1.917	2.895	3.190	3.577	3.724
Cr	0.003	0.0015	0.002	0.002	0.003	0.003	0.003	0.003	0.001	0.001	0.001
Fe^{3+}**	4.088	3.711	3.745	3.649	2.799	2.507	2.019	1.195	0.803	0.362	0.203
Mg	0.007	0.008	0.048	0.045	0.035	0.025	0.020	0.015	0.053	0.182	0.083
Ca	5.903	5.979	6.279	6.015	5.806	6.036	5.799	5.761	5.908	5.995	5.998
Mn	0.021	0.105	0.009	0.003	0.061	0.048	0.107	0.150	0.043	0.012	0.014
Al + Cr + Fe^{3+}	4.154	4.029	4.244	4.159	3.963	4.099	3.939	4.093	3.994	3.940	3.928
Ca + Mg + Mn	5.931	6.092	6.336	6.063	5.902	6.109	5.926	5.926	6.004	6.189	6.095
Components (mol%)**											
Uv	0.1	0.04	0.05	0.05	0.08	0.07	0.1	0.1	0.02	0.02	0.03
An	98.4	92.1	88.2	87.7	70.6	61.2	51.3	29.2	20.1	9.2	5.0
Gr	1.0	6.0	10.8	11.4	27.7	37.6	46.5	67.9	78.3	87.6	93.4
Py	0.1	0.1	0.8	0.74	0.6	0.4	0.3	0.3	0.9	2.9	1.4
Sp	0.3	1.7	0.1	0.06	1.02	0.8	1.8	2.5	0.7	0.2	0.2

* The mean and standard deviation are reported.
** The algorithm used for our microprobe program provides for some Fe^{2+} (by filling the dodecahedral site before filling the octahedral site).
† In the recalculation, all Fe was assumed to be Fe^{3+}. See text for discussion.

Santa Rita Peak garnets by Lager et al. (1989), it is probable that sample 25 has more OH, with ~0.4–2.9 wt% H_2O (estimated using extinction coefficients appropriate to grossular). For comparison, absorptivities were calculated from our reflectivity data. Intense absorptions were seen at 3553 and 3597 cm^{-1} in the OH stretching region of sample 25 (Fig. 1). The intensity pattern and peak positions are similar to those observed for samples from the same locality (Lager et al., 1989) and to those observed for two other andradite samples (Armbruster and Geiger, 1993). OH stretching bands were not resolved for any of our other samples: Figure 1 shows the spectrum for sample 27, which is typical. It appears that the low H_2O contents (less than about 0.4 wt% H_2O) previously measured for garnets from these localities (Rossman and Aines, 1991) are difficult to detect from reflectivity measurements. The H_2O content for sample 25 obtained from the calculated reflectance (Fig. 1) using the calibration of Rossman and Aines (1991) for grossularite was absurdly high, 18 wt% H_2O, compared with the content of 1.4 wt% H_2O surmised from the microprobe analysis of this andradite (its An content is 88%, Table 2). The extinction coefficient for OH in andradite is possibly an order of magnitude larger than that in grossularite. Given the bimodal appearance of the OH spectra (strong OH peaks for sample 25 vs. negligible absorptions for the others), the lack of a suitable calibration for OH in andradite, and the problematic chemistry of sample 25, we decided that it was not worthwhile to pursue further measurements of the sample's OH signature.

Site occupancies were assumed to be as follows: (1) For simplicity, Ti was assigned to the tetrahedral site. The Ti

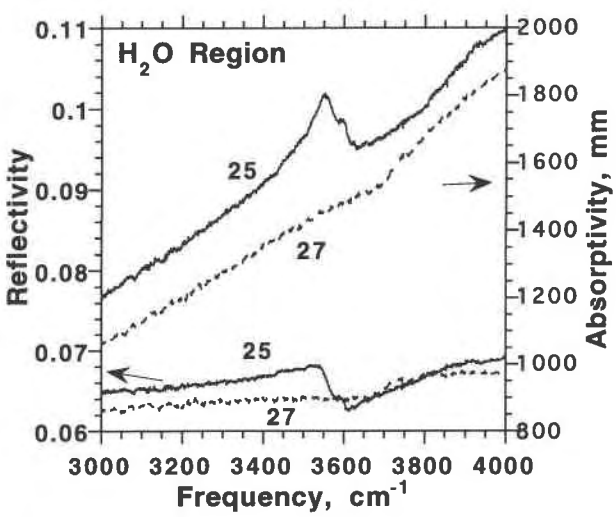

Fig. 1. Single-crystal reflectance spectra and calculated absorptivities in the near-IR region for representative samples. Solid line, sample 25. Dotted line, sample 27.

may be located in the octahedral site with Al in the tetrahedral site for charge compensation (e.g., Dowty, 1971; Deer et al., 1982; Huggins et al., 1977a, 1977b; Schwartz et al., 1980); however, for the low TiO_2 contents encountered here (about one-half of the samples have between 0.4 and 0.8 wt%, and the remainder have below 0.1 wt%), partitioning of Ti among any of the sites negligibly affects the recalculation. (2) All Fe was assumed to be Fe^{3+} in the octahedral site, except in the case of a few samples with overfilled octahedral sites (discussed below). Fe^{2+} was not determined from spectral measurements because we were not equipped to measure Fe^{2+} d-d transitions near 1000 nm. High concentrations of Fe^{2+} are not suggested by the color; the yellow-green color of grandites is due to Fe^{3+}, whereas the dark brown and orange colors of hand specimens are associated with high Mn contents (G. R. Rossman, 1993 personal communication). Speciation as exclusively Fe^{3+} appears reasonable for most samples because the dodecahedral site is filled by the divalent cations Ca, Mg, and Mn (Table 2). Samples 43, 25, 41, and 27 could have some Fe^{2+} because the octahedral site is overfilled in comparison with the dodecahedral site (Table 2). If we set the sum of Al + Cr + Fe^{3+} equal to 4 and assign excess Fe to the dodecahedral site, then the An contents of the three Fe-rich samples change negligibly (for sample 43, An becomes 98.35 mol% instead of 98.42; for sample 41, An becomes 87.25 mol% instead of 87.73; and for sample 25, An becomes 87.53 mol% instead of 88.24). However, allowing for Fe^{2+} for the Fe-poor sample 27 changes the An content from 29.20 to 27.55 mol%.

The samples (Table 2) are close to the grossular-andradite binary. To arrive at the binary compositions of Table 1, the uvarovite and andradite contents of Table 2 were summed. This approximation is reasonable because all samples contain <0.03 wt% Cr_2O_3 and because Cr and Fe are similar in mass. Also, pyrope, almandine, and spessartine contents were added to the grossular content of Table 2 to arrive at the binary representation of Table 1. The approximation of our series as $(Ca^{2+},Mn^{2+},Mg^{2+},Fe^{2+})_3Al_2Si_3O_{12}Ca_3(Fe^{3+},Cr^{3+},Al)_2Si_3O_{12}$ is reasonable because the sums of the pyrope, almandine, and spessartine components are all <3.1 mol%, and most are below 1.5 mol% (although sample 27 could have up to 5.7 mol% if Fe^{2+} is truly present), and because the focus of this study is on Al-Fe substitution in the octahedral site.

The effect of impurities on our spectral data and the above uncertainties in site occupancy will be accounted for in the subsequent analysis.

Optical properties

All samples are birefringent (Table 1). The degree varies by two orders of magnitude: δ ranges from 0.0004 to 0.01. The values for the birefringence are comparable to previous measurements (see summary by Meagher, 1982). The Darwin garnets are biaxial (Foord and Mills, 1978; Eastman, 1980); however, for most of the other samples an optical figure was difficult to see because of the spatial variation of the birefringence. Complex optical textures have been previously reported (Akizuki, 1984), including bow-tie patterns (Allen and Buseck, 1988). Thus, the optical properties of these samples appear to be typical of grossular-andradite.

A weak dependence of birefringence on composition is indicated for this suite. Grossular-rich samples have the lowest values, δ = 0.0004–0.001; andradite-rich garnets have moderate values, δ = 0.001–0.0050; and samples near the midpoint of the binary have the highest birefringences, δ = 0.0100 (see Table 1; Foord and Mills, 1978; Kingma and Downs, 1989). This correlation is tentative owing to the small number of samples investigated.

Results

IR reflectance spectra

All 14 garnet samples examined have intensity patterns (Fig. 2) characteristic of IR reflectance spectra for silicate garnets (cf. Hofmeister and Chopelas, 1991). [Spectra of samples 19 and 12 are found in McAloon and Hofmeister (1993). These are not repeated here because they are nearly the same as those of samples 24 and 43.] All 17 IR bands expected from symmetry analysis are observed in andradite-rich samples (sample 43 has 15 strong bands and two shoulders), whereas 15 obvious modes and one weak shoulder (at 425 cm^{-1}) are seen in grossular-rich samples. Peaks are labeled according to the nomenclature of Tarte (1965) and Moore et al. (1971).

The weak peaks in Figure 2 were confirmed in far-IR powder absorbance spectra. These data are not shown because no new features were revealed. Similarly, single-crystal absorbance spectra previously obtained from samples 12 and 19 (McAloon and Hofmeister, 1993) also agree with the reflectivity spectra of these samples.

The signal-to-noise ratio of the reflectance spectra is generally very high (Fig. 2). The small amount of noise seen in most spectra near 100 cm^{-1} is due to low absolute transmission near the spectral limits of the detector and beamsplitter. The spectrum of sample 19 is noisy near 600–650 cm^{-1} because a small area was sampled during acquisition of mid-IR data. Noise below 200 cm^{-1} for sample 41 is the result of diffraction because the sample's 100 μm dimension is near the wavelengths of the impinging light.

The dielectric functions obtained through Kramers-Kronig analysis (Fig. 3) are well behaved (see, e.g., the ideal cases presented by Wooten, 1972) and similar to those measured previously for garnets.[1] Figure 3 shows representative cases and the samples for which the intensity patterns varied the most. The andradite-rich samples (43, 19, and 33) have dielectric functions that are similar

[1] A copy of Figure 3 in its entirety may be obtained from the authors upon request. It may also be ordered as Document AM-95-601 from the Business Office, Mineralogical Society of America, 1015 Eighteenth Street NW, Suite 601, Washington, DC 20036, U.S.A. Please remit $5.00 in advance for the microfiche.

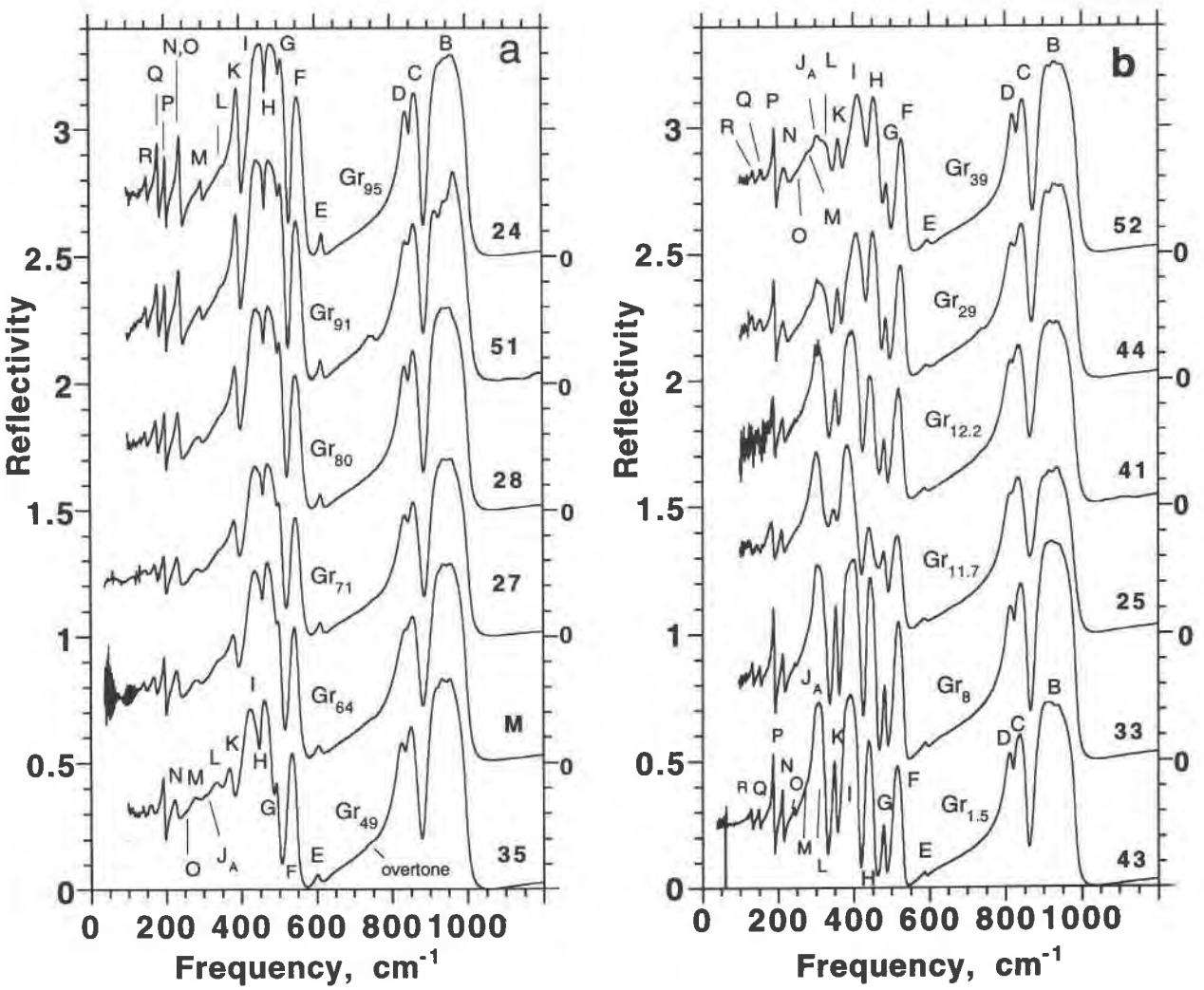

Fig. 2. Single-crystal reflectance spectra for grossular-rich (**a**) and andradite-rich (**b**) binary samples. Grossular (Gr) content (center) is given for each sample number (far right). Fundamental modes are labeled for representative samples. Noise is present in some spectra near 100, 200, or 600 cm^{-1}.

to those of sample 25 but with sharper peaks. The grossular-rich samples (28, 51, 24, and 12) have dielectric functions that are similar to those of sample 27 but with sharper peaks. Spectra from samples 12, 19, and M shown in McAloon and Hofmeister (1993) are not repeated here. Their dielectric functions are similar to those of samples 24, 43, and 35, respectively.

All samples between 8 and 92 mol% Gr display a feature near 750 cm^{-1}. This feature is probably an overtone because combinations of lower frequency fundamentals in affected samples are found yielding such a feature. In sample 27, for example, possible combinations are 407 + 351 = 758, 381.8 + 381.8 = 763.6, 461.8 + 290.2 = 752.0, and 611.8 + 151.5 = 763.3 cm^{-1}; similar combinations hold for the other samples as well. For sample 51, the peak at 758 cm^{-1} is more intense than is generally expected for an overtone. However, overtones superimposed on the stretching peaks near 900 cm^{-1} are also very intense for this garnet. The amount of impurity ions may enhance the resonances given that sample 51 has the strongest combination bands and the highest sum of pyrope and spessartine contents (3.1%), whereas the other samples that show strong combination peaks (samples 27 and 35) have the second highest sums (2.8 and 2.1%).

Sample 25 has an overtone at 672 cm^{-1}, but this peak appears to be the result of a different set of combinations, e.g., 368 + 292 = 660, 343 + 326 = 669, and 432 + 250 = 682 cm^{-1}; thus, the overtone of sample 25 should not be compared with those of the remaining samples.

Compositional dependence of IR modes

For the most part, the intensity pattern gradually changes from that of andradite to that of grossular (Figs. 2 and 3). Different peaks are affected to varying degrees. Specifically, the high-frequency stretching modes are little affected. Peaks near 400–500 cm^{-1} become better sepa-

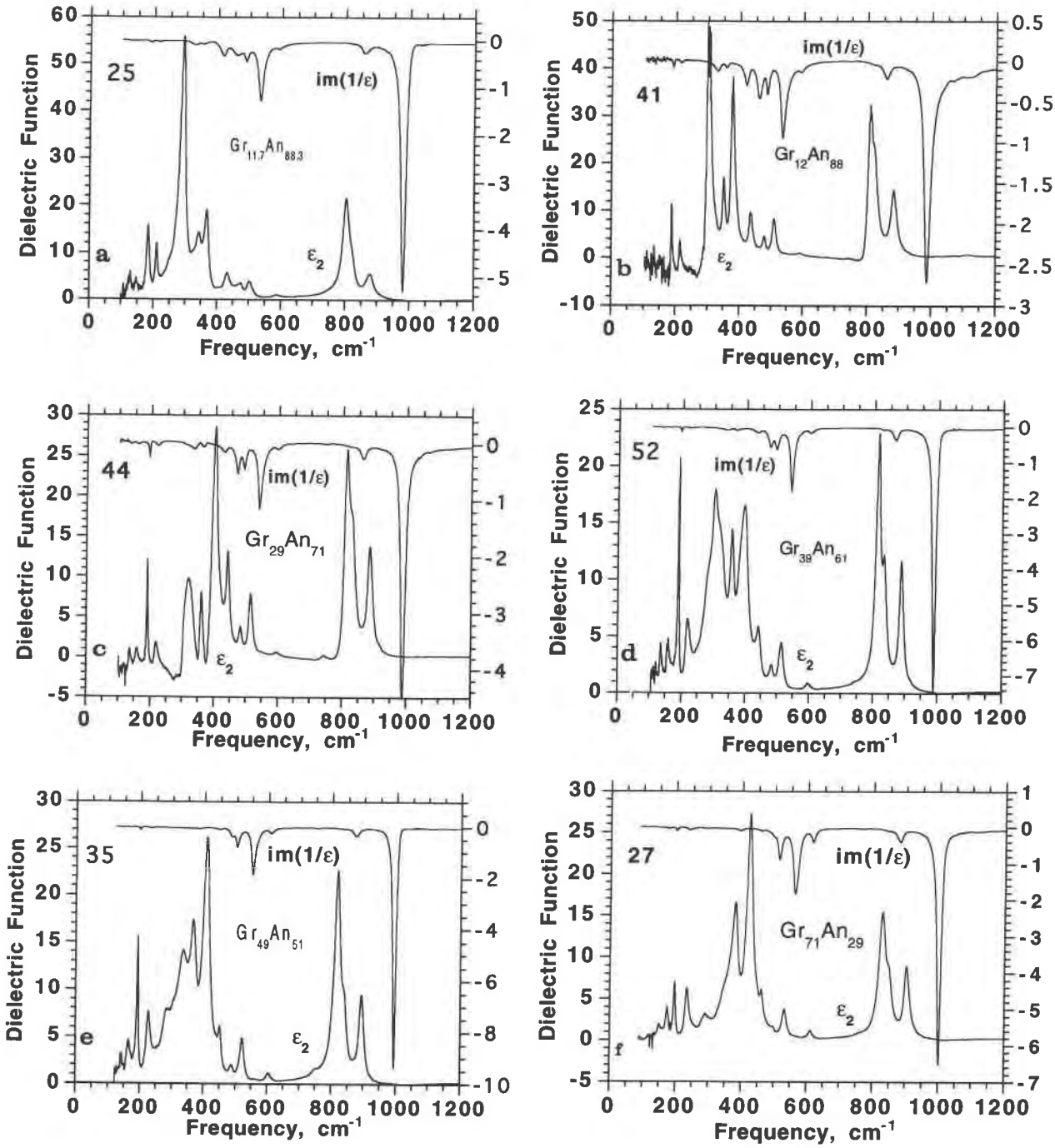

Fig. 3. The dielectric functions ϵ_2 and imaginary parts im(1/ϵ) of the grossular-andradite samples. Grossular (Gr) content is given for each sample number (upper left). Sample numbers 12, 19, and M can be seen in McAloon and Hofmeister (1993). Sample numbers 12, 24, 51, 28, M, 33, 19, and 43 have been deposited.

rated as the An content increases. Intensity generally increases near 300–375 cm^{-1} from sample 35 (49% Gr) to andradite. Intensity of the low-frequency peaks decreases from grossular to the middle of the binary and then increases again. Two modes (J_A and O) decrease in intensity as Gr content increases, eventually disappearing near the middle of the binary. Another very weak mode (J_G) is present in grossular but cannot be traced completely across the binary. We attempted to quantify the above relationships from both the raw data (Fig. 2) and the dielectric functions (Fig. 3) but did not find a strong correlation between relative or absolute intensity and composition.

Table 3. High-frequency IR peak positions (cm^{-1}) of $Ca_3(Fe,Al)_2Si_3O_{12}$ garnets

Mode		B		C		D		Overtone		E		F	
Assignment*		ν_3		ν_3		ν_3				ν_4		ν_4	
Sample	Normalized comp. (% Gr)	LO	TO	LO	TO	LO	TO	LO	TO	LO	TO	LO	TO
43	1.5	981.7**	879.7	819.5	825.2	857.9	807.4			590.7	589.5	531.9	506.1
19	6	988.0	884.6	823.8	830.5	861.6	811.9			594.6	590.7	536.1	510.6
33	8	983.6	880.3	822.4	826.3	860.8	806.7			593.2	592.0(0.2)	533.9	507.5
25	11.7†	980.5	879.9	821.0	~818	859.5	804.3	671	672.7(0.3)	590.6	588.5	533.6	502.7
41	12.2†	987.8	883.7	819.5	821.0	859.5	810.7	745	744	591.3	590.0(0.5)	536.0	509.1
44	29	988.7	886.4	827.4(0.5)	829.3(0.5)	863.2	813.7	743.8(0.3)	743.9	597.5	596.0	540.3	514.8
52	39	989.4	888.2	828.3	833.2	865.9	814.9	745.5(0.2)	746	600.2	597.8	541.8	514.6
35	49	994.5	893.8	836.3	837.5(0.5)	873.8	818.3	751.2	751.1(0.2)	607.9	604.5	551.3	521.9
M (Munam)	64	1000.3	900.3	~841	841.0	878(2)	825.6	752.4	752.3	612(2)	607.8	558.4	529.2
27	71	1001.0	903.5	845	846.1(0.5)	880.5	829.5	758.7(0.2)	758.0(0.5)	615.9	611.8	562.8	532.4
28	80	1001.0	902.4	846.1	848.5	880.9	829.3	758.5(0.2)	758.6	617.6	613.2	566.5	532.9
51	91	1007.8	903.9	849.1(0.5)	850(1)	882.7	833.2	758.7	757.8	620.1	614.9	572.4	536.3
24	95	1004.9	905.4	850.0	854.0	883.7	835.1			622.2	617.0	574.6	538.8
12	99	1007.4	907.8	851.4	856.3	884.7	837.7			623.8	618.0	576.2	539.8

* Assignments are based on those for grossular by Hofmeister and Chopelas (1991), where ν_3 is the asymmetric stretching motion of the SiO_4 tetrahedron, and ν_4 is the asymmetric bending motion of the SiO_4 tetrahedron.

** The uncertainty in the last digit is ±1 unless indicated differently.

† More figures are reported than are significant to differentiate samples 25 and 41.

The intensities display a zig-zag pattern with composition (not shown) possibly because of changes in mixing of modes across the binary.

Peak positions (Tables 3–5) increase almost uniformly with grossular content. Least-squares analyses indicate that the TO mode frequencies depend linearly on grossular content (Fig. 4). Thus, frequency also depends linearly on Al or Fe content or on the $Al/(Al + Fe^{3+})$ ratio. The slopes range from 0.18 to 0.69 cm^{-1}/mol% Gr, but most lie near 0.3 cm^{-1}/mol% Gr (Table 6). The highest slopes as well as the greatest departures from nonlinearity occur for the closely spaced, intense bands near 250–450 cm^{-1}, which probably interact and hence are mixed modes. The three peaks that cannot be traced completely across the series (J_A, J_G, and O) also depend linearly on composition.

Sample 25 at 11.7 mol% Gr lies below the trends of virtually all peaks. The much lower frequencies of this sample compared with those of sample 41, with similar grossular content (12.2 mol%), are seen both in the dielectric functions obtained from Kramers-Kronig analyses (Fig. 3) and in the raw data (Fig. 2). Sample 25 apparently includes a substantial hydrogarnet substitution as shown in the near-IR spectrum (Fig. 1) and because the amount of Si detected does not fill the site (Table 2). The amount of OH^- cannot be quantified from spectroscopy because to our knowledge an appropriate calibration is not available. We attribute the lower frequencies for sample 25 to its departure from the grossular-andradite binary. In particular, the OH^- substitution serves to expand the lattice, even for percent-level concentrations (see, e.g., Lager et al., 1989, and the following discussion). Hence the observed low frequencies for sample 25 are consistent with a significant hydrogarnet substitution.

Some of the remaining samples could also have tetrahedrally coordinated Al or Fe^{3+} or dodecahedrally coordinated Fe^{2+}, and thus their compositions may not be correctly represented by the approximations in Table 1. Some of the departures from linearity in Figure 4 could result from differences between the true and assumed site occupancies.

Discussion and conclusions

Two-mode behavior

For some solid solutions, IR peak positions vary smoothly with composition along the series much like the Vegard law behavior in X-ray diffraction (one-mode behavior). In other solid solutions, bands appear that are characteristic of each end-member. These may vary in peak position, but the main change is in relative intensity with composition along the series (two-mode behavior). Two-mode behavior originates in local modes and is expected if substantial differences exist between the masses of substituting ions or between the force constants (Chang and Mitra, 1968) and if end-member bands do not overlap (Fertel and Perry, 1979). In complex structures (e.g., perovskites) some bands may exhibit one-mode behavior while other bands exhibit two-mode behavior (Barker et al., 1968). Two-mode behavior was reported for translations of the SiO_4 tetrahedron in solid solutions between grossular and pyrope (or almandine) garnet (Hofmeister and Chopelas, 1991) and for the stretching modes and translations of the tetrahedra for solid solutions between $Y_3Al_2Al_3O_{12}$ and $Mn_3Al_2Si_3O_{12}$ (Lu et al., 1993).

For grossular-andradite solid solutions, large mass differences between Al and Fe could cause two-mode behavior. The disappearances of modes O, J_A, and J_G as composition progresses are compatible with two-mode behavior. The two higher frequency and higher intensity peaks constitute one pair. Mode O in andradite-rich compositions is probably correlated with mode N in grossu-

TABLE 4. Intermediate frequency IR peak positions (cm^{-1}) of $Ca_3(Fe,Al)_2Si_3O_{12}$ garnets

Mode Assignment*		G ν_4		H T(oct)		I ν_2	
Sample	Normalized comp. (% Gr)	LO	TO	LO	TO	LO	TO
43	1.5	484.3†	477.4	455.9	431.6	415.6	374.4
19	6	488.3	480.3	461.3	435.2	419.9	378.6
33	8	486.8	479.0	462.4	434.0	421.4	375.8
25	11.7‡	488.1	473.7	460.6	432.7	417.1	368.0
41	12.2‡	486.8	478.9	461.6	436.5	420.5	377.7
44	29	470.4	482.9	429.3	442.6	491.1	400.6
52	39	473.7	483.5	434.5	441.7	493.9	396.1
35	49	485.3	488.7	447.7	451.2	501.5	408.3
M (Munam)	64	494	494.3	456.9	459.2	510.8	419.8
27	71	497	494.1	458.9(0.2)	461.8	513.9	424.1
28	80	498	498	462.4	464.3	518.3	425.7
51	91	502.1	501.6(0.2)	465.2	467.0	523.5	431.8
24	95	503.8	503.8	467.8	469	526.2	433.9
12	99	506.0	506.0	469.5	470.6	529.4	434.9

* Assignments are based on those for grossular by Hofmeister and Chopelas (1991), where ν_4 is the asymmetric bending motion of the SiO_4 tetrahedron, ν_2 is the symmetric bending motion of the SiO_4 tetrahedron, T(oct) is a translation of the octahedrally coordinated cations against the O sublattice, and R(SiO_4) is a rotation-libration of the SiO_4 tetrahedron.
** The J mode has two components (two-mode behavior); see text.
† The uncertainty in the last digit is ±1 unless indicated differently.
‡ More figures are reported than are significant to differentiate samples 25 and 41.

lar, which was inferred to be a doublet from comparison with the other aluminous garnets (Hofmeister and Chopelas, 1991). All other peaks follow classical one-mode behavior. The reason for different behavior of the various modes in garnet is explicit in the band assignments, as discussed in the following sections.

Band assignments

Assignments of the observed IR peaks to atomic motions are based on symmetry analysis (Moore et al., 1971), previous IR data on chemical substitutions among garnets (Hofmeister and Chopelas, 1991), and our data (which directly link andradite and grossular peaks). The correlation of Figure 4 requires that previous assignments (Hofmeister and Chopelas, 1991) for modes H, I, K, N, R, Q, P, and O in andradite be revised (Tables 4 and 5). The old assignments were made by pairing peaks in grossular and andradite, which was difficult because two peaks are missing for grossular. The connection of IR peaks to atomic motions is a first approximation in which mode mixing is assumed to be negligible. We do not imply that the contributions of atomic motions from individual sites in garnet represent localized vibrations.

Two-mode behavior (discussed above) is observed for two bands only. This behavior is consistent with assignment of these particular bands (J and O) to translations of the octahedral cation (Tables 4 and 5). Other motions predicted by symmetry analysis lack the requisite large

TABLE 5. Low-frequency IR peak positions (cm^{-1}) of $Ca_3(Fe,Al)_2Si_3O_{12}$ garnets

Mode Assignment*		M T(SiO_4)		O T(oct)		N T(dod)		P T(dod)		Q T(dod)		R T(SiO_4)**	
Sample	Normalized comp. (% Gr)	LO	TO	LO	TO	LO	TO	LO	TO	LO	TO	LO	TO
43	1.5	279(2)†	280(2)	245.4	244.7	214.7	212.7	190.7	187.3	151.9	151.1	132.3	131.4
19	6	~284	~279	247.5	246.4	216.7	214.0	192.1	188.4	154.2	153.0	134.7	133.7
33	8		280	?	246.9(0.3)	216.6	213.9	192.1	188.0	154.1	153.3	134.8	133.8
25	11.7‡	274(2)	268(2)	255(2)	~250	214.5	211.3	189.3	184.2	148.7	148.2	129.7	129.1
41	12.2‡	300	275	250(2)	248.6	216.2	215.3	191.2	189.0	152.0	151.8	135.2	134.8
44	29	292	287	255	~254	220.7	218.8	194.1	190.1	158.9	158.4	136.4	135.8
52	39	293	284.0			225.3	220.2	195.2	190.9	161.1	160.3	138.3	136.6
35	49	291(2)	287(2)			231.8	226.7	197.2	193.2	167.0	165.3	144.5	142.8
M (Munam)	64	292.8	288.5			238.3	232.7	200.5	197.0	175.0	172.4	147.6	146.7
27	71	291.9(0.5)	290.2			239.7	234.2	200.4	197.4	177.0	174.6	151.8	151.5
28	80	296.5	293.8			243.0	236.0	203.0	199.8	180.4	177.5	152.0	150.3(0.3)
51	91	299.0	298.0			245.7	239.5	204.3	202.2	183.9	181.5	153.7	153.0
24	95	301.1	299.2			247.0	240.6	205.9	203.5	186.6	183.4	155.7	154.6
12	99	302.9	300.6	248.7§	241.4§	248.7§	241.4§	207.4	204.5	188.8	184.0	157.5	155.6

* Assignments are based on those for grossular by Hofmeister and Chopelas (1991), where T(oct) indicates a translation of the cations in the octahedrally coordinated site, T(dod) indicates translations of the cations in the dodecahedral interstice, and T(SiO_4) indicates a translation of the tetrahedron.
** This mode is probably mixed with T(dod).
† The uncertainty in the last digit is ±1 unless indicated differently.
‡ More figures are reported than are significant to differentiate samples 25 and 41.
§ Inferred to be a doublet.

TABLE 4.—*Continued*

Mode Assignment*	J_G** T(oct)		K R(SiO_4)		L R(SiO_4)		J_A** T(oct)	
Sample	LO	TO	LO	TO	LO	TO	LO	TO
43			355.4	348.1	322	321.5(0.5)	329.0	297.7
19			359.5	351.6	323	324.0	332.5	301.0
33			359.9	350.5		324.7(0.5)	332.8	296.9
25			353.9	343.2	330	326(2)	324.6	292.4
41			358.0	351.5	~323	~322	330.0	~302
44	400(2)	383	364.3	360.0	335.9	319.8	310(2)	305.4
52		384(2)	368.3	357.9	339.3	~325	312(1)	303.9
35		~390	379.9	366.8	346.3	335.9	327(2)	317(2)
M (Munam)		~400	390.6	377.4	354(2)	345.9	332(2)	314.1
27	433(2)	~407	393.0	381.8	353	351(2)		
28		~412	396.4	383.6	353(2)	349.7		
51	438(2)	~416	400.0	388.4	356(1)	357(1)		
24	441(2)	~419	402.8	390.0	355.8	355.7		
12	450(2)	425(2)	404.9	389.8	356.0	355.0		

mass or force-constant difference in the grossular-andradite series. Symmetry analysis predicts that three translations involving the octahedral site should occur. The third octahedral translation (mode H at 432 cm^{-1} in andradite and 471 cm^{-1} in grossular) does not meet the criteria of nonoverlapping peaks because the end-member peaks overlap (if the dependence of frequency on lattice constant is accounted for).

Frequency, composition, and structure

Frequency depends on atomic mass, bond length, and the strength of the chemical bond. In a series, the change in the bond strength should be gradual and dependent on the bond length. Hence, the observed, approximately linear dependence of frequency on composition (Fig. 4) should be related to structural changes in the series be-

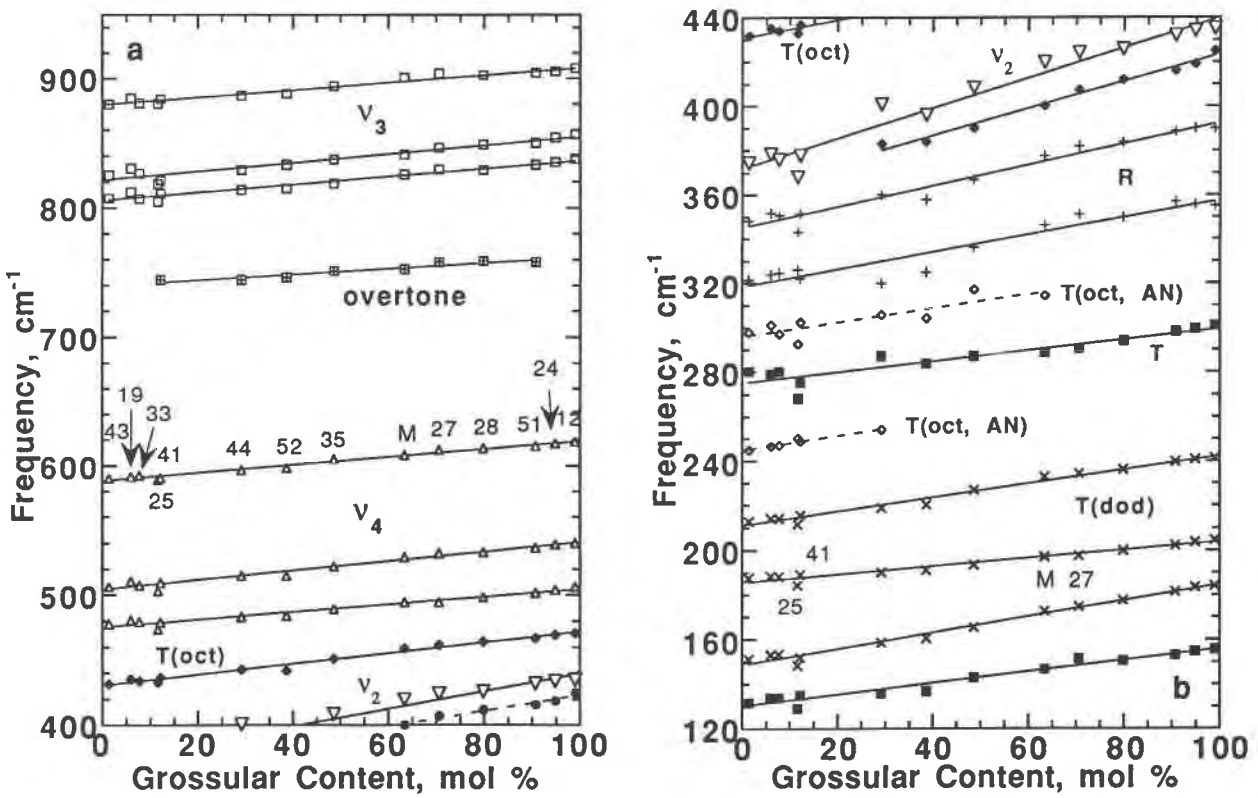

Fig. 4. IR frequencies of grossular-andradite fundamental TO modes as a function of composition. Uncertainties in frequency are smaller than the symbol. (**a**) High-frequency modes. (**b**) Low-frequency modes. Symbols: open squares = ν_3, squares with crosses = overtone, upward pointing triangles = ν_4, solid diamonds = T(oct), downward pointing triangles = ν_2, solid circles = T(Al), open diamonds = T(Fe), plus signs = R, solid squares = T, Xs = T(dod). Least-squares fits are shown as solid lines for bands exhibiting one-mode behavior or dashed lines for two-mode behavior. Small labels are sample numbers.

TABLE 6. Linear representation* of grossular-andradite IR modes

Mode	Assignment	ν_0 (cm^{-1})	$d\nu/dX$ (cm^{-1}/mol% Gr)	R
B	ν_3	879.3	0.300	0.98
C	ν_3	821.3	0.334	0.96
D	ν_3	805.3	0.313	0.98
Overtone		739.4	0.223	0.95
E	ν_4	587.7	0.311	0.99
F	ν_4	504.2	0.363	0.98
G	ν_4	475.0	0.293	0.98
H	T(oct)	430.5	0.413	0.99
I	ν_2	371.8	0.679	0.98
J_G	T(Al)	362.2	0.611	0.99
K	R	345.1	0.472	0.98
L	R	318.4	0.391	0.95
J_A	T(Fe^{3+})	295.6	0.317	0.87
M	T	275.1	0.244	0.92
O	T(Fe^{3+})	244.6	0.334	0.97
N	T(dod)**	210.7	0.316	0.99
P	T(dod)	185.5	0.181	0.98
Q	T(dod)	148.4	0.362	0.99
R	T	130.1	0.258	0.98

* These parameters were obtained from least-squares analysis: ν_0 is the grossular position, $d\nu/dX$ is the slope, and R is the goodness of fit.
** For Gr-rich samples this peak is probably degenerate with T(Al).

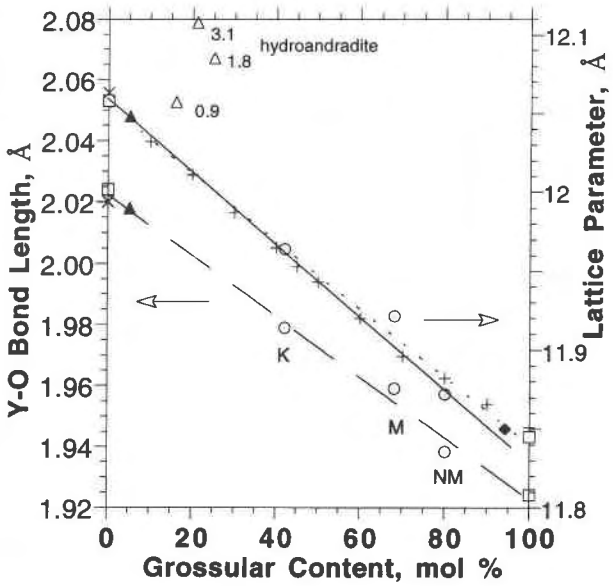

Fig. 5. Summary of crystallographic data on grossular-andradite. Symbols: open squares = single-crystal data from Novak and Gibbs (1971); open circles = single-crystal data from Takeuchi et al. (1982), labeled as K = Kamaishi, M = Munam, and NM = North Moravia; solid diamond = single-crystal data from Allen and Buseck (1988); solid triangles = single-crystal data from Kingma and Downs (1989); plus signs = powder data of Huckenholz et al. (1974); open triangles = single-crystal data on hydrous Santa Rita andradite by Lager et al. (1989). Open triangles are labeled with their OH contents (as wt% H_2O, determined from X-ray refinements). Dashed and dotted lines are least-squares fits to all the data. (Allen and Buseck, 1988, did not report Y-O bond lengths.) The solid line is the trend defined by andradite-rich samples.

cause the mass difference directly influences only three modes and is accounted for in the existence of two-mode behavior.

Most of the existing crystallographic data on grossular-andradite garnets (Fig. 5) are derived from powder diffractometry of synthetic samples. The compositions are thus precise, but the data do not include bond lengths. Several single-crystal studies involve birefringent garnets, and most of these refinements utilized lower symmetry space groups. The variation in space group presents no obstacle in the comparison of measurements because the reduced-symmetry unit cells were metrically cubic or could be closely approximated by a pseudocubic cell. The study of Santa Rita andradite (Lager et al., 1989) produced lattice constants differing considerably from the series (Fig. 5). The data suggest that the lattice constant of sample 25 is at least as large as that of end-member andradite, which is consistent with the measured values for its frequencies (Fig. 4). The OH contents of the two Santa Rita Peak samples shown are estimated as 0.4 and 2.9 wt% H_2O (Lager et al., 1989), such that the more hydrated sample has the larger lattice constant. The trend clearly indicates the strong influence of OH on the structural parameters of garnets.

Least-squares analysis of all garnets except the San Benito samples shows that the cubic lattice parameter varies roughly linearly with composition (Fig. 5). The fit gives

$$\text{lattice parameter (Å)} = 12.055 - 0.00215 \cdot \text{Gr content (mol\%)} \quad (3)$$

with a goodness of fit equal to 0.997. The departure from linearity in Figure 5 may be associated with the compositions of the garnets of Takeuchi et al. (1982) lying slightly off the binary because the Munam sample, which is situated farthest from the trend, has the largest amounts of impurities (Mn, Ti, and Fe^{2+}). The degree of ordering does not correlate well with the departure from linearity because the most highly ordered sample (Kamaishi garnet) lies on the line (Fig. 4). The crystallographic data appear compatible with a slight difference in slope between andradite- and grossular-rich compositions. Frequency vs. composition may also show a slight flattening near the grossular end-member. Thus, it appears that frequency correlates directly with the lattice parameter and that the relationship is approximately linear.

Cation-O bond lengths (such as those of the octahedra shown in Fig. 5) may depend linearly on grossular content. However, the data are not sufficient to establish a relationship, and therefore it is premature to attempt a correlation of frequency with bond lengths.

The linear correlation between IR peak positions and composition of grandite garnets allows estimation of composition from vibrational spectra, given that the garnet in question is determined to be a grandite (and not significantly hydrated) using an independent method (e.g., color, association, or semiquantitative chemical analysis). The most reliable indicator modes are the peaks that are both well resolved and fairly intense, e.g., modes B or F. If powder measurements are made, the far-IR modes

would serve well as tracers because the absorption frequencies of these weak modes lie close to the TO component, and thus particle size and scattering affect the far-IR modes the least.

Chemical bonding

The frequencies of the Fe local modes in grossular should be related to the Al modes either by $(m_{Al}/m_{Fe})^{1/2} = 0.688$, assuming the cations vibrate against the O sublattice, or by $(\mu_{Al-O}/\mu_{Fe-O})^{1/2} = 0.897$, assuming the O anions participate (μ is reduced mass). (By comparing the local modes, we eliminate the need to consider bond lengths.) The observed ratios are 0.776 for mode J couple, 1.14 for mode O-N couple, and 1.00 for mode H (which follows one-mode behavior). Two of the Fe modes (O and H) have higher frequencies than expected, suggesting that their bond strengths are larger. The larger intensity for the translations of Fe^{3+} in andradite in comparison with the Al translations in grossular also suggests stronger chemical bonding of Fe. This can probably be explained by the fact that the larger Fe ion fills the octahedral site more fully.

Mixing properties

The observed, approximately linear dependence of the vibrational frequencies on composition (and similar behavior for the lattice parameters) suggests that thermodynamic properties such as heat capacity and entropy follow ideal mixing laws because these quantities are integrals of various functions involving the vibrational frequencies (Kieffer, 1979). This inference agrees with conclusions of previous workers (e.g., Holdaway, 1972; Ganguly, 1976; Perchuk and Aranovich, 1979; Bird and Helgeson, 1980) that grossular-andradite behaves essentially as an ideal ionic solution.

Similarly, bulk moduli calculated using the vibrational data for this series in Hofmeister's (1991) model would also vary linearly with composition. The predicted linear dependence differs considerably from the inference of a minimum near 22 mol% grossular (Bass, 1986). Even if we account for the slight departures in frequency and lattice parameter from a linear relationship with composition, the resultant calculated minimum would still be less than one-tenth as deep as that observed. We propose that the observed minimum in bulk modulus, which is defined by only one sample, is an artifact resulting from the variance of that particular sample's composition from the binary. The sample in question is a black andradite with 2.69 wt% TiO_2 (Babuska et al., 1978). Ti^{4+} is probably octahedrally coordinated, with Al in the tetrahedra to provide charge compensation. This large amount of Ti (and substitution of Al for Si) is sufficient to alter the vibrational frequencies (note that sample 25 of the present study with a smaller Si deficiency, Table 2, has frequencies that are lower than the linear trend of Fig. 4). The black color of Babuska's sample indicates that intervalence charge transfer is occurring, and thus the bonding may also differ for the garnet in question. Not only could these differences affect compressibility, but also this particular sample is so far off the binary that it simply should not be used to establish mixing properties.

Birefringence in grossular-andradite

Optical anomalies are present in the suite investigated here (Table 1), as are commonly observed for grossular-andradite (Meagher, 1982). Yet, our IR data are compatible with the cubic garnet structure. One possibility is that the IR spectra are not sensitive to the Al-Fe ordering inferred from the crystallographic refinements (Takeuchi et al., 1982; Allen and Buseck, 1988; Kingma and Downs, 1989) but visible measurements are. The higher sensitivity in the visible could be related to differences in chemical bonding because the metal-O charge transfer that occurs in the ultraviolet has a tail into the visible region. However, we favor the hypothesis that ordering may not be present (symmetry reduction should have increased the number of IR bands) and strain causes the birefringence as discussed by McAloon and Hofmeister (1993). (For a discussion of hypotheses other than strain or ordering, see Meagher, 1982.) The relationship of structural strain to composition is discussed in detail by Armbruster and Geiger (1993); in particular, they observed that the same amount of strain is present in *I*1 as in *Ia*3*d* garnets. In addition to the previous arguments, the ideal mixing previously observed (e.g., Ganguly, 1976; Bird and Helgeson, 1980) and inferred in this work may not be compatible with the degrees of ordering of up to 65% reported for the intermediate compositions (Takeuchi et al., 1982).

Acknowledgments

We heartily thank F. Allen (Engelhard Corporation, New Jersey), P. Buseck (Arizona State University), J. DeMouthe (California Academy of Sciences, San Francisco), H.S. Eastman (Bond Gold Company, Colorado), A.R. Kampf and D.L. Eatough (Los Angeles County Natural History Museum), K. Kingma (Johns Hopkins University), J. Downs (Ohio State University), and G.R. Rossman (California Institute of Technology) for their help in providing samples. We also thank T. Fagan, S. Roeske, and R. Schaal (University of California, Davis) for obtaining microprobe data. Many thanks also to N. Winter (University of California, Davis) for help in sample preparation. B.P.M. wishes to thank P. Kelly (University of California, Davis) for helpful comments and discussion. E. Libowitsky (California Institute of Technology), G.A. Lager (University of Louisville), and H. Skogby (Swedish Museum of Natural History) are thanked ville), and H. Skogby (Swedish Museum of Natural History) are thanked for helpful reviews. Support was provided by the David and Lucile Packard Foundation.

References cited

Akizuki, M. (1984) Origin of optical variations in grossular-andradite garnet. American Mineralogist, 69, 328–338.

Allen, F.M., and Buseck, P.R. (1988) XRD, FTIR, and TEM studies of optically anisotropic grossular garnets. American Mineralogist, 73, 568–584.

Andermann, G., Caron, A., and Dows, D.A. (1965) Kramers-Kronig dispersion analysis of infrared reflectance bands. Journal of the Optical Society of America, 55, 1210–1216.

Armbruster, T., and Geiger, C.A. (1993) Andradite crystal chemistry, dynamic X-site disorder and structural strain in silicate garnets. European Journal of Mineralogy, 5, 59–71.

Babuska, V., Fiala, J., Kumazawa, M., Ohno, I., and Sumino, J. (1978) Elastic properties of garnet solid-solution series. Physics of the Earth and Planetary Interiors, 16, 157–176.

Barker, A.S., Jr., Ditzenberger, J.A., and Guggenheim, H.J. (1968) Long-wavelength optical lattice vibrations in mixed $KMgF_3$-$KNiF_3$ crystals. Physical Review, 175, 1180–1190.

Bass, J.D. (1986) Elasticity of uvarovite and andradite garnets. Journal of Geophysical Research, 91, 7505–7516.

Bird, D.K., and Helgeson, H.C. (1980) Chemical interactions of aqueous solutions with epidote-feldspar mineral assemblages in geologic systems: I. Thermodynamic analysis of phase relations in the system CaO-FeO-Fe_2O_3-Al_2O_3-SiO_2-H_2O-CO_2. American Journal of Science, 280, 907–941.

Chang, I.F., and Mitra, S.S. (1968) Applications of a modified long-range iso-displacement model to long-wavelength optic phonons of mixed crystals. Physical Review, 172, 924–933.

Deer, W.A., Howie, R.A., and Zussman, J. (1982) Rock-forming minerals, vol. 1A: Orthosilicates, 919 p. Longman, London.

Dowty, E. (1971) Crystal chemistry of titanian and zirconian garnet: I. Review and spectral studies. American Mineralogist, 56, 1983–2009.

Eastman, H.S. (1980) Skarn genesis and sphalerite-pyrrhotite-pyrite relationships at the Darwin Mine, Inyo County, California. Ph.D. thesis, Stanford University, Stanford, California.

Fertel, J.H., and Perry, C.H. (1979) Optical phonons in $KCl_{1-x}Br_x$ and $K_{1-x}Rb_xI$ mixed crystals. Physical Review, 184, 874–884.

Foord, E.E., and Mills, B.A. (1978) Biaxiality in 'isometric' and 'dimetric' crystals. American Mineralogist, 63, 316–325.

Ganguly, J. (1976) The energetics of natural garnet solid solutions: II. Mixing of the calcium silicate end-members. Contributions to Mineralogy and Petrology, 55, 81–90.

Ganguly, J., and Saxena, S.K. (1987) Mixtures and mineral reactions, 291 p. Springer-Verlag, Berlin.

Hofmeister, A.M. (1991) Calculation of bulk moduli and their pressure derivatives from vibrational frequencies and mode Grüneisen parameters: Solids with cubic symmetry or one-nearest-neighbor distance. Journal of Geophysical Research, 96, 16181–16203.

Hofmeister, A.M., and Chopelas, A. (1991) Vibrational spectroscopy of end-member silicate garnets. Physics and Chemistry of Minerals, 17, 503–526.

Holdaway, M.J. (1972) Thermal stability of aluminum-iron epidote as a function of f_{O_2} and iron content. Contributions to Mineralogy and Petrology, 36, 307–340.

Huckenholz, H.G., Lindhuber, W., and Springer, J. (1974) The join $CaSiO_3$-Al_2O_3-Fe_2O_3 of the CaO-Al_2O_3-Fe_2O_3-SiO_2 quaternary system and its bearing on the formation of grandite garnets and fassaitic pyroxenes. Neues Jahrbuch für Mineralogie Abhandlungen, 121, 160–207.

Huggins, F.E., Virgo, D., and Huckenholz, H.G. (1977a) Titanium-containing silicate garnets: I. The distributrion of Al, Fe^{3+}, and Ti^{4+} between octahedral and tetrahedral sites. American Mineralogist, 62, 475–490.

——— (1977b) Titanium-containing silicate garnets: II. The crystal chemistry of melanites and schorlomites. American Mineralogist, 62, 646–665.

Kerr, P.F. (1977) Optical mineralogy, 492 p. McGraw-Hill, New York.

Kieffer, S.W. (1979) Thermodynamics and lattice vibrations of minerals: III. Lattice dynamics and an approximation for minerals with application to simple substances and framework silicates. Reviews in Geophysics and Space Physics, 17, 35–39.

Kingma, K.J., and Downs, J.W. (1989) Crystal-structure analysis of a birefringent andradite. American Mineralogist, 74, 1307–1316.

Lager, G.A., Armbruster, T., Rotella, F.J., and Rossman, G.R. (1989) OH substitution in garnets: X-ray and neutron diffraction, infrared, and geometric-modeling studies. American Mineralogist, 74, 840–851.

Lu, R., Jackson, K.D., and Hofmeister, A.M. (1993) Thin-film infrared spectra from solid solutions of spessartine and yttrium aluminum garnet. Canadian Mineralogist, 31, 381–390.

McAloon, B.P., and Hofmeister, A.M. (1993) Single-crystal absorption and reflection infrared spectroscopy of birefringent grossular-andradite garnets. American Mineralogist, 78, 957–967.

Meagher, E.P. (1982) Silicate garnets. In Mineralogical Society of America Reviews in Mineralogy, 5, 25–66.

Moore, R.K., White, W.B., and Long, T.V. (1971) Vibrational spectra of the common silicates: I. The garnets. American Mineralogist, 56, 54–71.

Novak, G.A., and Gibbs, G.V. (1971) The crystal chemistry of the silicate garnets. American Mineralogist, 56, 791–825.

Perchuk, L.L., and Aranovich, L.Y. (1979) Thermodynamics of minerals of variable compositions: Andradite-grossularite and pistacite-clinozoisite solid solutions. Physics and Chemistry of Minerals, 13, 1–14.

Rossman, G.R., and Aines, R.D. (1991) The hydrous component in garnets: Grossular-hydrogrossular. American Mineralogist, 76, 1153–1164.

Schwartz, K.B., Nolet, D.A., and Burns, R.G. (1980) Mössbauer spectroscopy and crystal chemistry of natural Fe-Ti garnets. American Mineralogist, 65, 142–153.

Takeuchi, Y., Haga, N., Umizu, S., and Sato, G. (1982) The derivative structure of silicate garnets in grandite. Zeitschrift für Kristallographie, 158, 53–99.

Tarte, P. (1965) Etude experimentale et interpretation du spectre infrarouge des silicates et germanates: Application a des problemes structurauz relatifs a l'etat solide. Memoires de l'Academie Royale de Belgique 35, no. 4(a), p. 1–259; no. 4(b) p. 1–134.

Wooten, F. (1972) Optical properties of solids, 260 p. Academic, San Diego, California.

Manuscript received November 28, 1994
Manuscript accepted July 31, 1995